Table S1: Swivel module rotations and backbone RMSD[1]

Swivel rotation to go from X to Y (models were pre-aligned based on RNAP core module) (also see Figure S6B)						
X \ Y	Backtrack40	Backtrack60	Pre-cleavage	Post-cleavage	Reactivated	EC (6ALH)
Backtrack40	0˚	3.9˚	no swiveling[2]	4.0˚	no swiveling[2]	1.2˚
Backtrack60		0˚	-3.4˚	no swiveling[2]	-3.9˚	-2.9˚
Pre-cleavage			0˚	2.8˚	no swiveling[2]	no swiveling[2]
Post-cleavage				0˚	-4.2˚	-3.1˚
Reactivated					0˚	1.5˚
EC (6ALH)						0˚
Backbone RMSD (aligned based on RNAP core module): above diagonal core, below diagonal swivel						
	Backtrack40	Backtrack60	Pre-cleavage	Post-cleavage	Reactivated	EC (6ALH)
Backtrack40	0	0.57	0.84	1.0	1.14	1.0
Backtrack60	3.19	0	0.86	0.91	1.24	0.94
Pre-cleavage	1.66	2.66	0	1.23	1.44	1.08
Post-cleavage	3.18	1.62	2.68	0	1.38	0.78
Reactivated	1.52	3.66	3.55	4.27	0	1.33
EC (6ALH)	1.57	2.53	2.17	2.36	1.74	0
Backbone RMSD of RNAP swivel module (aligned based on swivel module)						
	Backtrack40	Backtrack60	Pre-cleavage	Post-cleavage	Reactivated	EC (6ALH)
Backtrack40	0					
Backtrack60	0.87	0				
Pre-cleavage	0.91	1.12	0			
Post-cleavage	1.1	1.19	1.21	0		
Reactivated	1.31	1.55	1.02	1.01	0	
EC (6ALH)	0.95	0.91	1.17	1.02	1.26	0

[1]all calculations were made with PyMOL

[2]no swiveling implies either no rotation or dominant rotation around different rotation axis

Table S2

Data collection	Backtracked non-swiveled	Backtracked swiveled	Pre-cleavage	Post-cleavage	Reactivated
Particles	268851		758120	270554	380141
Pixel size (Å)	1.067		1.1	1.04	1.04
Defocus range (um)	0.8 – 3.2		0.8 – 3.2	0.8 – 3.2	0.8 – 3.2
Voltage (kV)	300		300	300	300
Electron dose (e^{-} Å^{-2})	49		51	59	45.6
Model composition					
Non-hydrogen atoms	26305		27299	28572	27183
Protein residues	3185		3321	3519	3363
RNA bases	13		13	10	10
DNA bases	59		48	59	53
Ligands (Zn^{2+}/Mg^{2+})	2/1		2/1	2/1	2/1
Refinement					
Final particles used	60080	102899	574584	121680	170328
Resolution (Å)	3.7	3.4	3.7	3.9	3.6
Map sharpening B-factor (Å^2)	118.5	130.7	184.7	169.3	135.4
Average B factor (Å^2)	174	152.4	101.1	203.9	134.2
RMS deviations					
Bond lengths (Å)	0.012	0.016	0.01	0.01	0.01
Bond angles (°)	1.1	1.3	1	1	1
Ramachandran plot					
Favored (%)	84.13	82.8	86.32	85.61	86.29
Allowed (%)	15.75	17.13	13.65	14.39	13.52
Outliers (%)	0.13	0.06	0.03	0	0.19
Molprobity					
Clash score	19.74	17.8	13.5	23	15.9
Rotamer outliers (%)	0.07	0.18	0.07	0.1	0.00
Overall score	2.47	2.45	2.27	2.5	2.3

Figure S1:

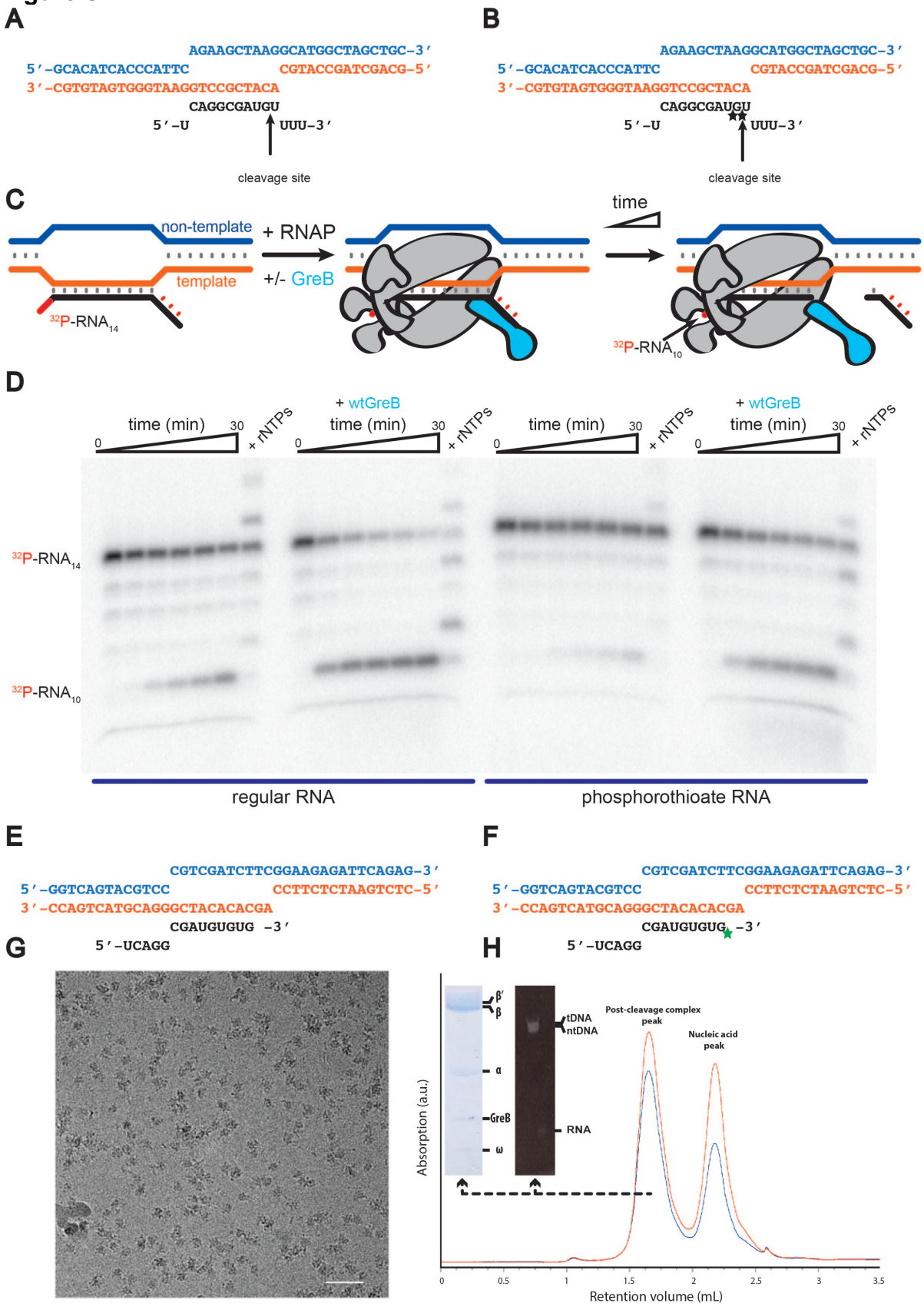

Figure S1. RNA-DNA scaffold schematics, RNA cleavage kinetics, and particle distribution. (A) Schematic diagram of the nucleic acids used to monitor RNA

cleavage and prepare samples for EM reconstructions. Non-template DNA (blue), and template DNA (orange) anneal with an RNA (black) that has three mismatched bases at the 3′-end. The cleavage site is indicated. About 15 different scaffold designs had to be tested to avoid cleavage at more than one position and resolve the backtracked RNA in the reconstruction (not shown). (B) Same as (A) but with the location of the phosphorothioate modifications indicated (black stars). (C) Schematic for cleavage assay. After complex formation, samples are taken at different time points to follow RNA cleavage. (D) Denaturing polyacrylamide gels of cleavage products show that GreB accelerates RNA cleavage (left). The resulting complex is active and resumes transcription (+NTPs). Using an RNA with phosphorothioate modifications slows down the cleavage without affecting the position (right). (E) Schematic of nucleic acids used to form post-cleavage and (F) substrate bound, reactivated complex. RNA containing a 3′-deoxy-rGMP (green star) was used to trap the complex before RNA extension. (G) Typical micrograph shows even particle distribution. (H) Size exclusion chromatography confirms the stability of the post-cleavage complex. Denaturing polyacrylamide gels confirm the presence of all components in peak fractions. All 4 complexes are stable enough for size exclusion chromatography (not shown).

Figure S2:

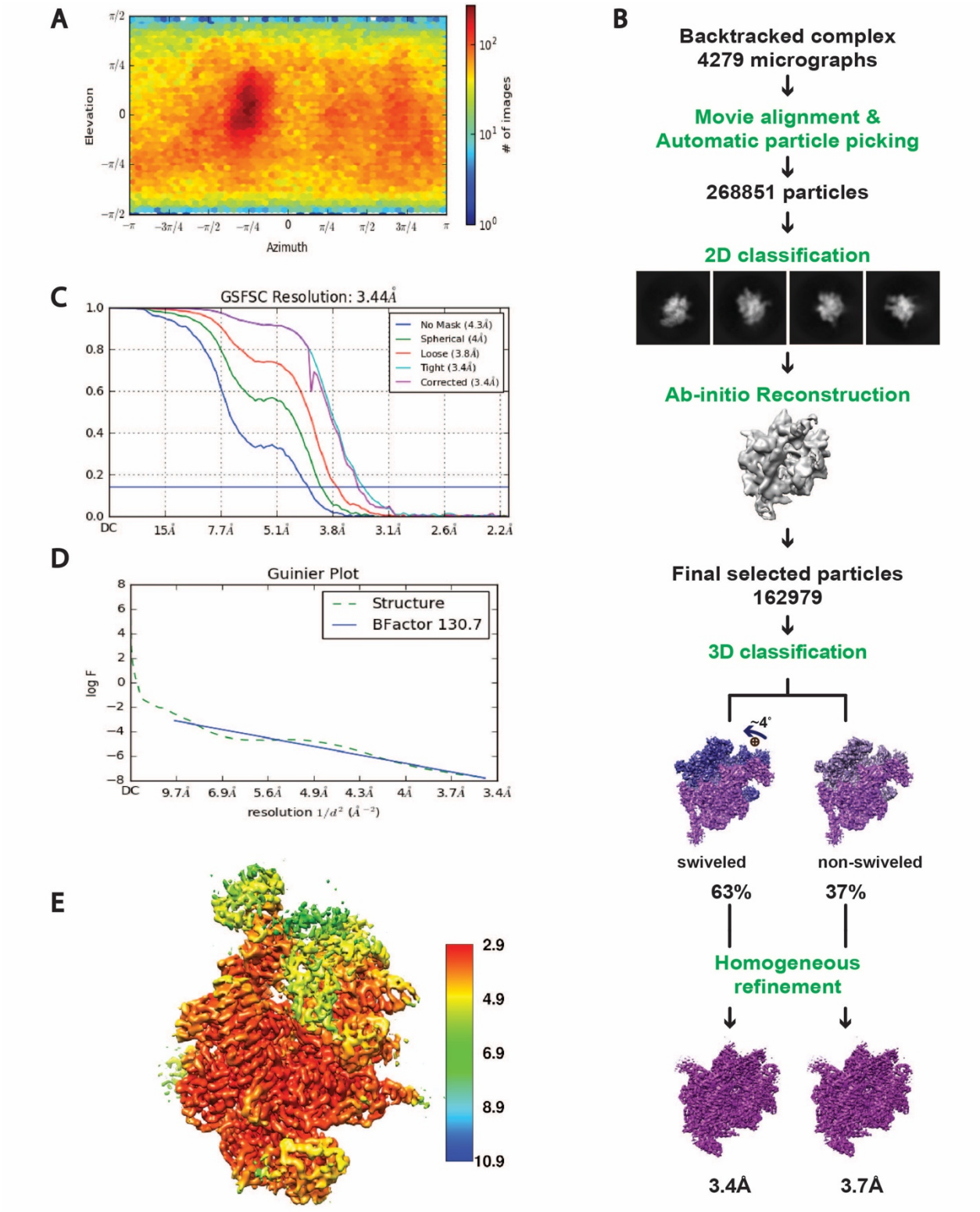

Figure S2. Refinement statistics and flow chart of Cryo-EM data processing for backtracked complex. (A) Distribution of particle orientation shows slight preferential orientation bias. (B) Processing and classification flow chart. 3D classification produced 2 classes, which differed in their swivel module orientation relative to RNAP

core. (C) Fourier shell correlation (FSC) plot for half-maps with 0.143 FSC criteria indicated. The nominal resolution is 3.4 Å for the swiveled complex. (D) The Guinier plot indicates a B-factor of about 130. (E) The core of the complex reaches below 3Å in local resolution but at the periphery the resolution is lower.

Figure S3:

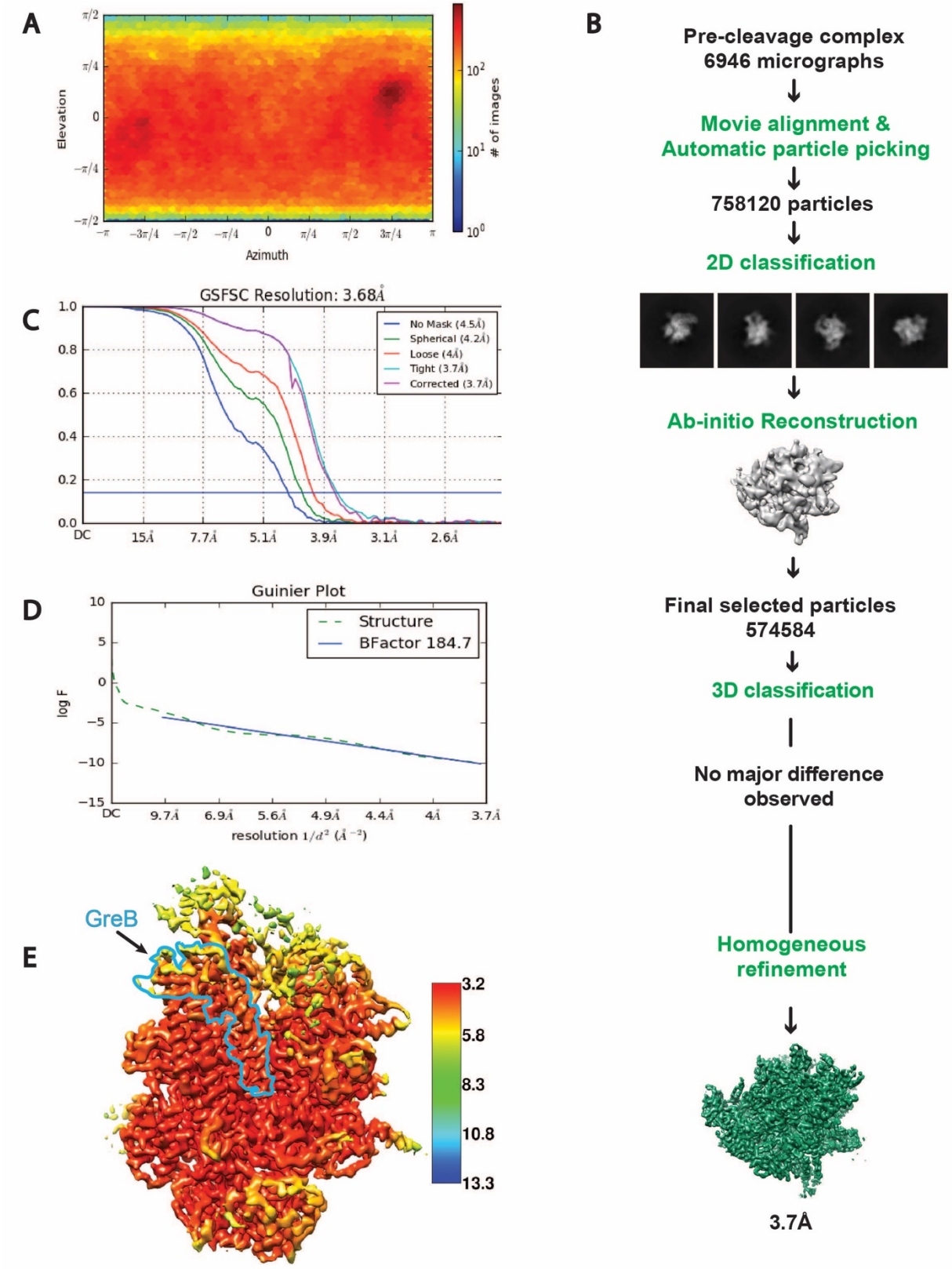

Figure S3. Refinement statistics and flow chart of Cryo-EM data processing for pre-cleavage complex. (A) Distribution of particle orientation shows slight preferential orientation bias. (B) Processing and classification flow chart. 3D

classification did not indicate any conformational heterogeneity. (C) Fourier shell correlation (FSC) plot for half-maps with 0.143 FSC criteria indicated. The nominal resolution is determined to be 3.7 Å. (D) The Guinier plot indicates a B-factor of about 185. (E) The core of the complex reaches close to 3.2Å in local resolution with slightly lower resolution at the periphery.

Figure S4:

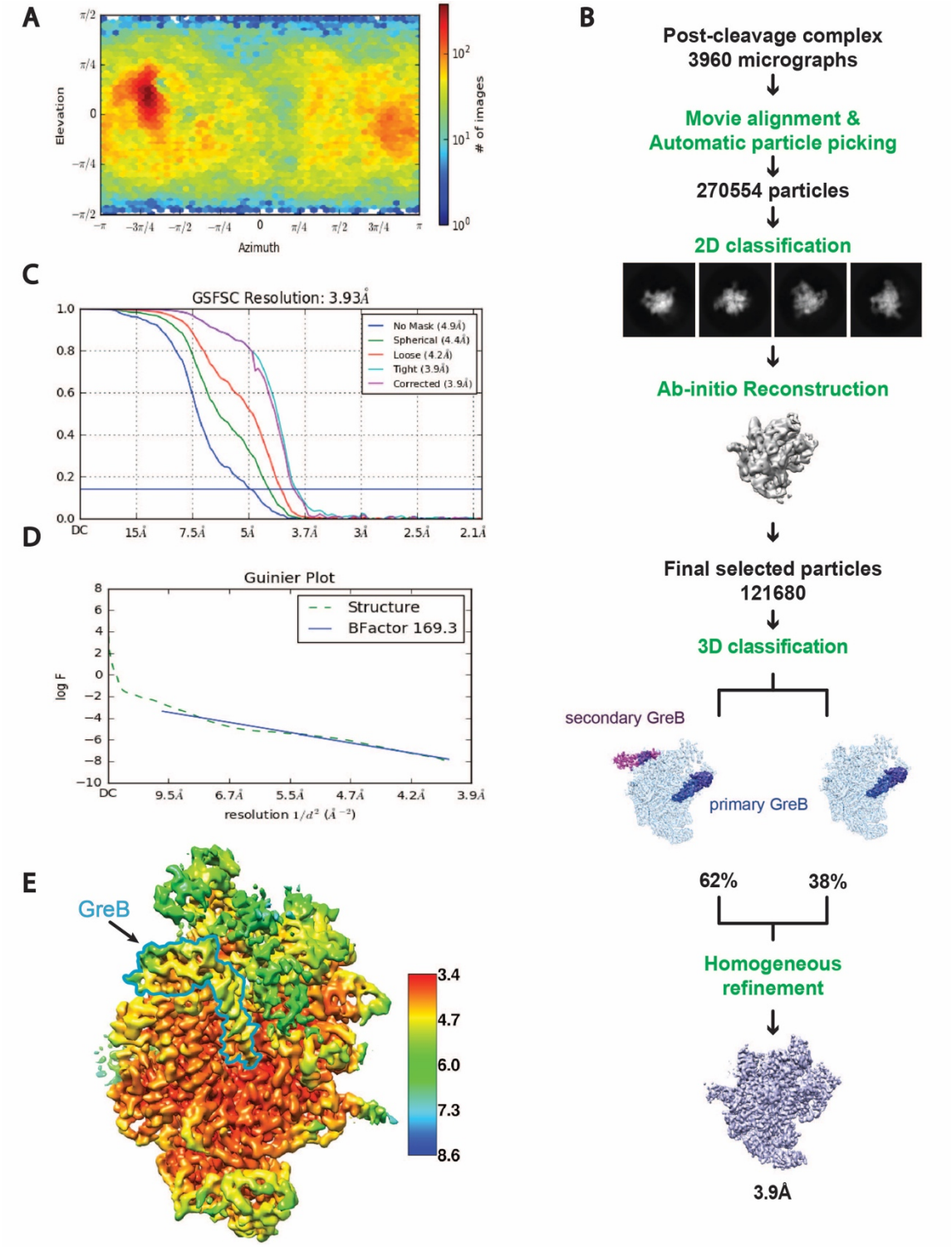

Figure S4. Refinement statistics and flow chart of Cryo-EM data processing for post-cleavage complex. (A) Distribution of particle orientation shows preferential orientation bias. (B) Processing and classification flow chart. 3D classification produced 2 major classes, which differed in the absence or presence of a second copy of GreB close to the upstream DNA. (C) Fourier shell correlation (FSC) plot for

half-maps with 0.143 FSC criteria indicated. The nominal resolution is determined to be 3.9 Å. (D) The Guinier plot indicates a B-factor of about 170. (E) The core of the complex reaches close to 3.4Å in local resolution but at the periphery the resolution is lower.

Figure S5:

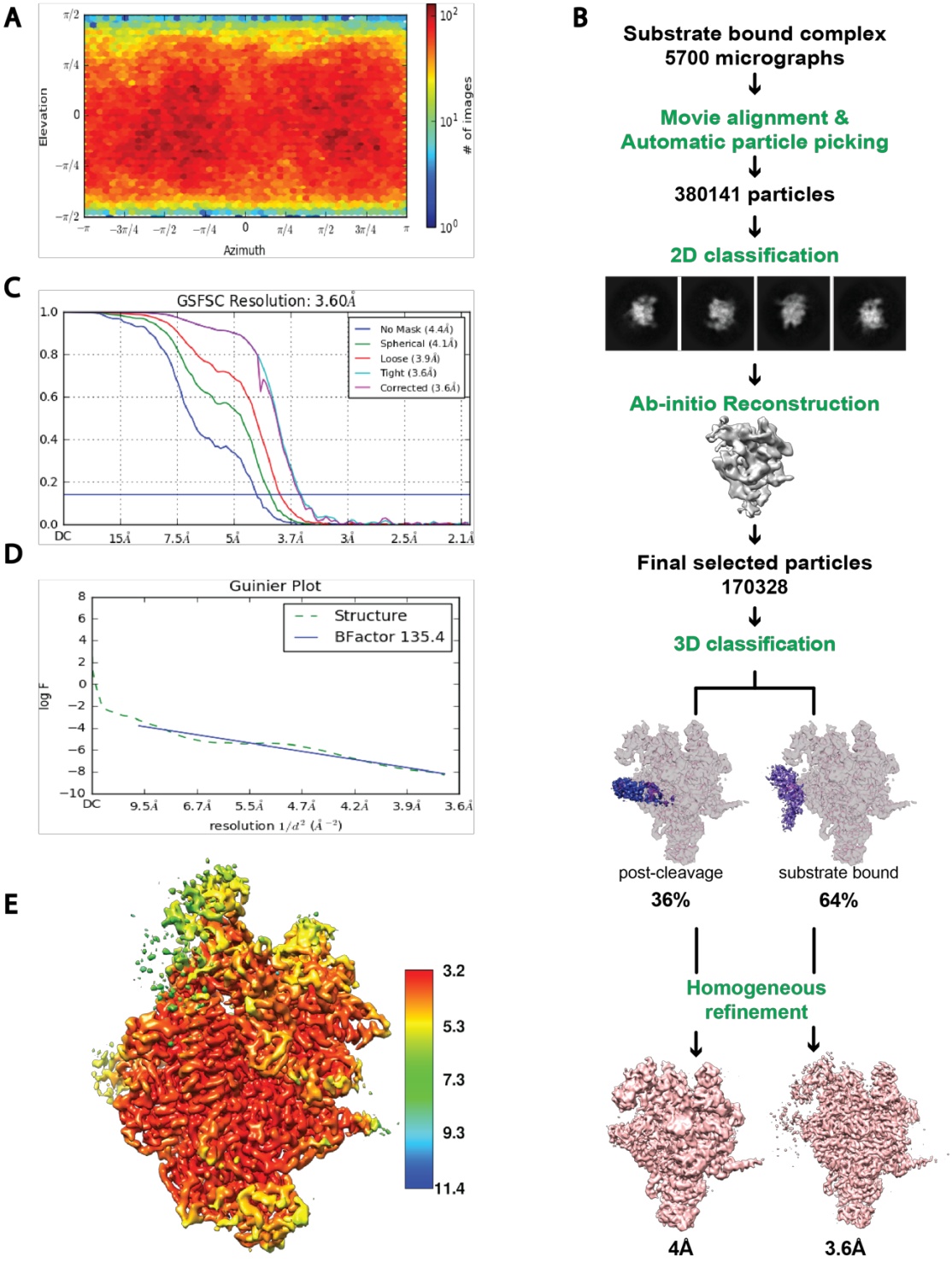

Figure S5. Refinement statistics and flow chart of Cryo-EM data processing for substrate bound, reactivated complex. (A) Distribution of particle orientation. (B) Processing and classification flow chart. 3D classification produced 2 major classes: 36% of particles represent a post-cleavage complex with GreB bound in the

secondary channel and no substrate in the active site. 64% of particles contain a substrate in the active site and GreB in the ejected, dislodged position on the surface of RNAP. (C) Fourier shell correlation (FSC) plot for half-maps with 0.143 FSC criteria indicated. The nominal resolution is determined to be 3.6 Å for the reactivated, substrate bound complex. (D) The Guinier plot indicates a B-factor of about 135. (E) The core of the complex reaches around 3.2Å in local resolution but at the periphery the resolution is lower.

Figure S6:

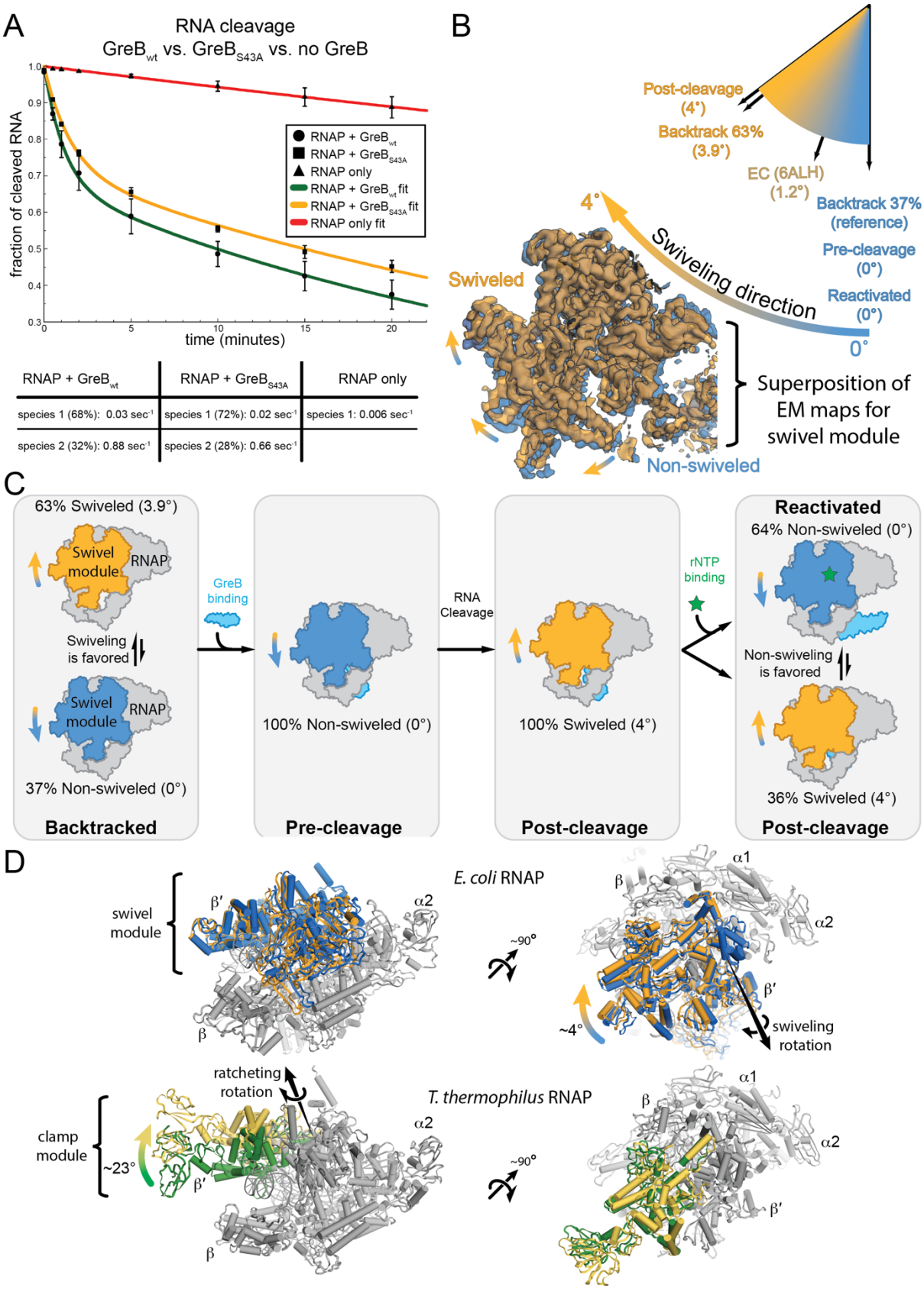

Figure S6. RNAP conformational dynamics during backtracking and reactivation. (A) Comparison of RNA cleavage kinetics. An S43A GreB mutant

exhibits slightly slower cleavage rates than the wildtype protein (orange vs. green curve). RNAP without GreB (red) is shown for comparison to illustrate the effect of GreB on RNA cleavage rates. (B) RNAP swivel movements. Schematic (top right) to show where the various states lie on the spectrum of observed swivel rotations (0˚, marine to 4˚, orange). The non-swiveled backtracked state serves as the reference. Superposition of the map for the swivel module (RNAP clamp and shelf domain) from the pre-, and post-cleavage complex illustrates difference and extent of movement. (C) Schematic to illustrate observed swivel module states in samples covering the reaction from backtracked state (left, both non-swiveled and swiveled RNAP present), pre-cleavage (non-swiveled only), post-cleavage (swiveled only), to reactivated sample (substrate-bound non-swiveled and GreB bound, post-cleavage, swiveled state). GreB interactions spanning SI3 and the backtracked RNA in the pre-cleavage complex versus lack of that interaction with backtracked RNA in the post-cleavage complex may contribute to the change in swiveling preference. (D) Comparison of swiveling observed for *E. coli RNAP* (top) and ratcheting observed for *Thermus thermophilus* RNAP (bottom). *T. thermophilus* RNAP and *E. coli* RNAP were aligned based on the RNAP core module and two identical views (left versus right column) are shown to illustrate that ratcheting and swiveling movements are different. The rotation axis for swiveling (top, right) and ratcheting (bottom, left) are indicated and adopt approximately a 45˚ angle. Swivel module for *E. coli* RNAP (top, blue or orange), clamp module for *T. thermophilus* RNAP clamp module (bottom, green or yellow), and RNAP subunits are labeled.

Movie S1. Overview of RNAP backtracking and reactivation. The movie gives an overview of RNAP conformational changes during the entire reaction from backtracking, through RNA cleavage and reactivation. First, we morph a canonical elongation complex to adopt the backtracked state. We show the two populations observed in the backtracked state (swiveled vs. non-swiveled) and zoom into the active site. Then GreB binding induces a change in SI3 leading to the pre-cleavage complex. A zoom of the active site shows the engaged GreB stabilized by the backtracked RNA. Cleavage of the RNA leads to the post-cleavage complex and we show the changes in the conformation of the GreB tip, which is now more disordered. Finally, substrate binding results in folding of the trigger helices and shift

of SI3 closing the secondary channel. GreB cannot insert into the active site anymore and is loosely bound on the surface.